

Article

Fatigue Performance Test and Numerical Analysis of Composite Girders with CSW-CFST Truss Chords

Hanhui Huang ¹, Kangming Chen ^{1,*}, Qingxiong Wu ¹ and Shozo Nakamura ²

¹ College of Civil Engineering, Fuzhou University, Fuzhou 350108, China; huanghh0603@163.com (H.H.); wuqingx@fzu.edu.cn (Q.W.)

² Department of Civil and Environmental Engineering, Nagasaki University, Nagasaki 852-8521, Japan; shozo@nagasaki-u.ac.jp

* Correspondence: chen-kang-ming@163.com; Tel.: +86-188-5014-9877

Abstract: Composite girders with corrugated steel webs and concrete-filled steel tubular (CSW-CFST) truss chords are a new type of structure and have been used in bridges. To study the fatigue performance of these composite girders, model tests and numerical analysis were conducted, and the results compared with those for composite girders with corrugated steel webs and steel tubular (CSW-ST) truss chords. The results indicated that concrete-filling the chords constrained chord radial deformation and relieved hot-spot stress in the intersecting weld zones of composite girders with CSW-ST truss chords by 18.5–60.1%. The crack growth rates along both depth and length directions in composite girders with CSW-CFST truss chords were lower than those of composite girders with CSW-ST truss chords during the crack propagation and failure stages. Under the same fatigue load, concrete-filling the chords increased the fatigue life of composite girders with CSW-ST truss chords by 61.5%. Under the condition that there is no fatigue design S-N curve, the fatigue design S-N curve given in API can be used to evaluate the fatigue life of composite girders with CSW-CFST truss chords with a deviation of less than 17.4%.



Citation: Huang, H.; Chen, K.; Wu, Q.; Nakamura, S. Fatigue Performance Test and Numerical Analysis of Composite Girders with CSW-CFST Truss Chords. *Appl. Sci.* **2022**, *12*, 5459. <https://doi.org/10.3390/app12115459>

Academic Editors: Junwon Seo and Jong Wan Hu

Received: 23 March 2022

Accepted: 26 May 2022

Published: 27 May 2022

Publisher's Note: MDPI stays neutral with regard to jurisdictional claims in published maps and institutional affiliations.



Copyright: © 2022 by the authors. Licensee MDPI, Basel, Switzerland. This article is an open access article distributed under the terms and conditions of the Creative Commons Attribution (CC BY) license (<https://creativecommons.org/licenses/by/4.0/>).

Keywords: composite girders; corrugated steel webs; concrete-filled steel tubular truss chords; fatigue performance test; numerical analysis; fatigue performance; evaluation method

1. Introduction

Due to the composite bridge, corrugated steel webs and concrete-filled steel tubular (CSW-CFST) chord (Figure 1a) have less torsion stiffness and a narrow space between the corrugated steel web and the CFST chord which is adverse to welding [1]. As a result, a new type of composite structure has been proposed [2], referred to as the composite girder with CSW-CFST truss chords (Figure 1b). The composite girder with CSW-CFST truss chords, which replace the concrete bottom slab and steel truss webs, has many advantages, including reducing the dead load, improving fatigue crack resistance [3], avoiding localized joint damage [4], and preventing buckling of steel chords subject to hogging moment by concrete-filling the chords [5]. Recently, the composite girder with CSW-CFST truss chords has been successfully applied in some bridges, as shown in Figure 2.

The research community has provided valuable and interesting results on the relevant static performance of composite girders with CSW-CFST truss chords. The shear lag effect in composite girders with CSW-CFST truss chords was investigated. The results showed that concrete-filling in the chord had little influence on the shear-lag effect [6]. A model test and numerical analysis of the torsion capacity of composite girders with CSW-CFST truss chords was carried out, and a simplified calculation formula for their torsion rigidity and resistance was presented [7]. The flexural capacity of continuous composite girders with CSW-CFST truss chords was tested [8]. The study analyzed the influences of the main structural parameters on flexural capacity, and found that the ultimate capacity of the

composite girder with concrete-filling in the chords was 1.22 times that without concrete-filling in the chords. The dynamic impact coefficient and live load correction coefficient of composite girders with CSW-CFST truss chords was researched [9]. The failure modes of composite girders with CSW-CFST truss chords under the combined action of bending and torsion stresses was investigated [10].

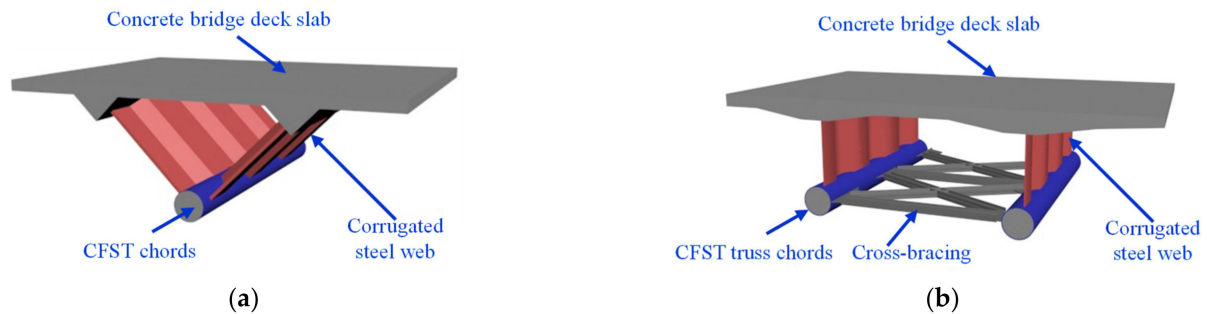


Figure 1. Composite girders: (a) CSW-CFST chords; and (b) CSW-CFST truss chords.

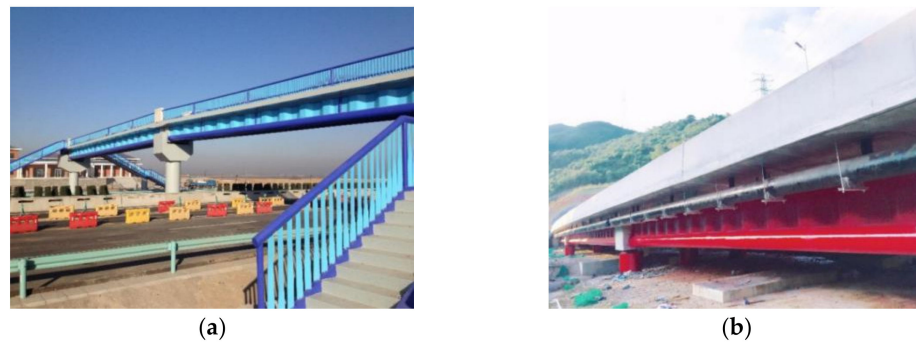


Figure 2. Photo of completed bridges: (a) a footbridge in Hebei Province, China; and (b) Maluanshan Park Viaduct in Guangdong Province, China.

While there is relatively mature theory relating to the statics of composite girders with CSW-CFST truss chords, practical engineering applications have not considered the fatigue performance, and no fatigue performance evaluation methods have been defined in design specifications. Currently, information about fatigue model tests and numerical analyses of composite girders with CSW-ST truss chords can only be found in [11], in which hot-spot stress distribution, fatigue failure modes, and fatigue life have been explored.

The research results above have demonstrated that concrete-filling in the chord could effectively improve the static properties, and existing studies [12–16] show that concrete-filling in the chord can improve the fatigue performance of the joints. However, previous fatigue testing has not involved full model testing but only testing of joints. Thus, to investigate the influence of concrete-filling in the chord on the fatigue performance of composite girders with corrugated steel webs and steel tubular (CSW-ST) truss chords, a fatigue performance test and numerical analysis were conducted in this study. The study focused on the extrapolation method and the distribution of hot-spot stress, the mechanism by which concrete-filling in the chord influences the fatigue performance, and fatigue failure modes. A fatigue life evaluation method for composite girders with CSW-CFST truss chords is proposed and discussed using the fatigue performance test results.

2. Model Test

2.1. Model Design

It has been found [8] that the dead load of a girder can increase by 8% because of concrete-filling the chord, while the bearing capacity can increase by 22%. Concrete-filling the chord can enhance the radial stiffness of the chord, which can reduce the thickness of the chord. Concrete-filling the chord involves more labor, more material consumption, higher

self-weight, and added uncertainties, but the advantages outweigh the disadvantages described above.

To analyze the influence of concrete-filling the chord on the fatigue performance of composite girders with CSW-ST truss chords, the model designed for this study adopted the same geometry and materials as composite girders with CSW-ST truss chords investigated in [11], except that the chord was filled with concrete. The scale of the test model was 1:5. Figure 3 shows the detailed dimensions. The total length and span between the supports of the test model were 9000 mm and 8760 mm, respectively. The height of the end cross beam and main girder cross-section were 600 mm and 560 mm, respectively. The width and thickness of the concrete bridge deck slab were 1700 mm and 100 mm, respectively. The steel grade used in the fatigue performance test was Grade Q345 steel [17]. These welds comprised full penetration welds, with the material properties of the welds needing to be consistent with the steel. The size of the welds was determined by reference to stipulations given in [17].

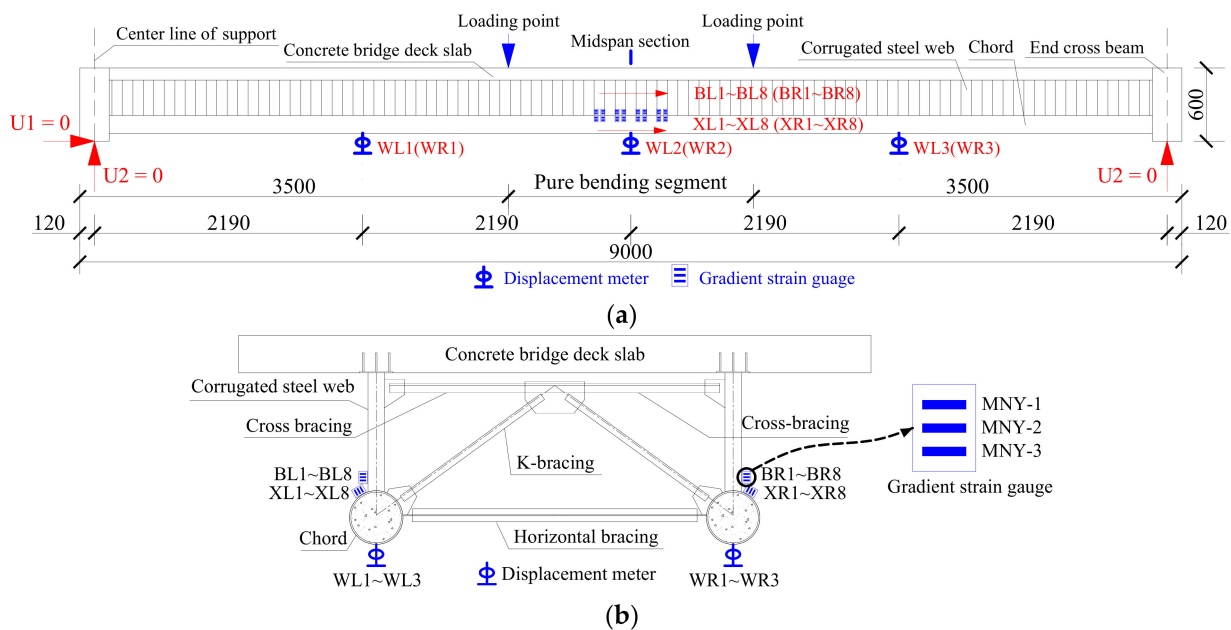


Figure 3. Scaled test model and layout of measurement points (unit: mm): (a) elevation; and (b) cross-section.

The detailed specifications of the chord, corrugated steel web, horizontal bracing, cross-bracing, and K-bracing are listed in Table 1. According to [18], the main geometric parameters of the corrugated steel web include the dip angle of the inclined web (θ_w), and the bend radius (R_w), thickness (T_w), wavelength (L_w), and wave height (H_w), as shown in Figure 4; the detailed dimensions of the corrugated steel web are shown in Table 1. The intersecting location of the inclined web and the arc transition segment is represented as point S.

Table 1. Summary of test model specifications.

Chord	K-Bracing	Horizontal Bracing	Cross-Bracing	Corrugated Steel Web				
				T_w	θ_w	L_w	H_w	R_w
Ø146 mm × 6 mm	L23 mm × 4 mm	L5 mm	L40 mm × 3 mm	4 mm	31°	320 mm	44 mm	60 mm

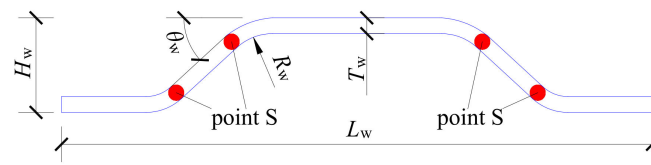


Figure 4. Key geometric parameters of corrugated steel web.

To facilitate analysis and exposition, the two sides of the intersecting weld between the corrugated steel web and the chord are referred to as the left- and right-hand-side, respectively, with the axial direction of chords understood as the forward direction according to the path direction of the corrugated steel web. The corrugated steel web was further divided into the mold-pressing side (indicate in red in Figure 5) and the non-mold pressing side (indicated in blue in Figure 5) with respect to the position of the fixed molding head.

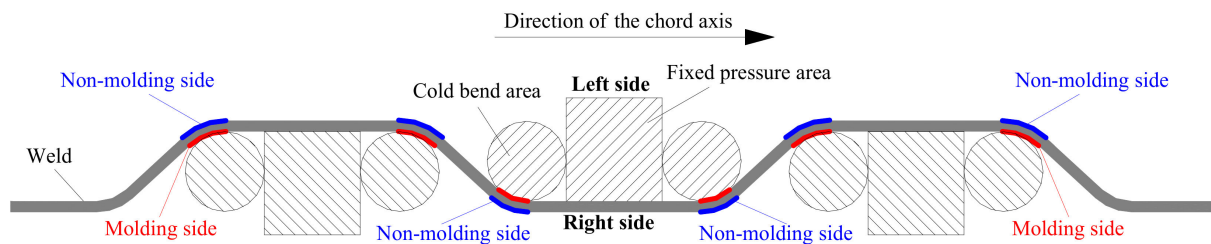


Figure 5. Locations of intersecting welds between corrugated steel web and chord.

The mechanical properties of the steel and concrete used in the test model were determined from experimental stress-strain curves. As shown in Tables 2 and 3, f_y, f_u, E_s and μ_s represent the yield strength, ultimate strength, modulus of elasticity and Poisson ratio of the steel structure, respectively. f_{ck}, f_{cd}, E_c and μ_c represent the axial compressive standard strength, axial compressive design strength, modulus of elasticity and Poisson ratio of the concrete structure, respectively.

Table 2. Mechanical properties of steel.

Component	f_y (MPa)	f_u (MPa)	E_s (GPa)	μ_s
Chord	348	491	204	0.3
K-bracing	361	457	203	0.3
Cross-bracing	349	482	199	0.3
Horizontal bracing	355	468	203	0.3

Table 3. Mechanical properties of concrete.

Concrete Grade	f_{ck} (MPa)	f_{cd} (MPa)	E_c (MPa)	μ_c
C50	34.7	26.2	35.2	0.2

2.2. Loading Method and Rig

The loading rig drawing and photo are shown in Figure 6a,b, respectively. The four-point loading method was adopted, in a similar way to the fatigue performance test of composite girders with CSW-ST truss chords reported in [11]. A very stiff load distribution beam was placed parallel to the test model, such that its mid-span coincided with that of the test model. Rubber bearings separated by 2000 mm were arranged at both ends of the distribution beam to ensure that it was in contact with the deck slab of the test model. A 500-kN MTS servo-loading system was used to apply vertical load at the mid-span of the distribution beam.

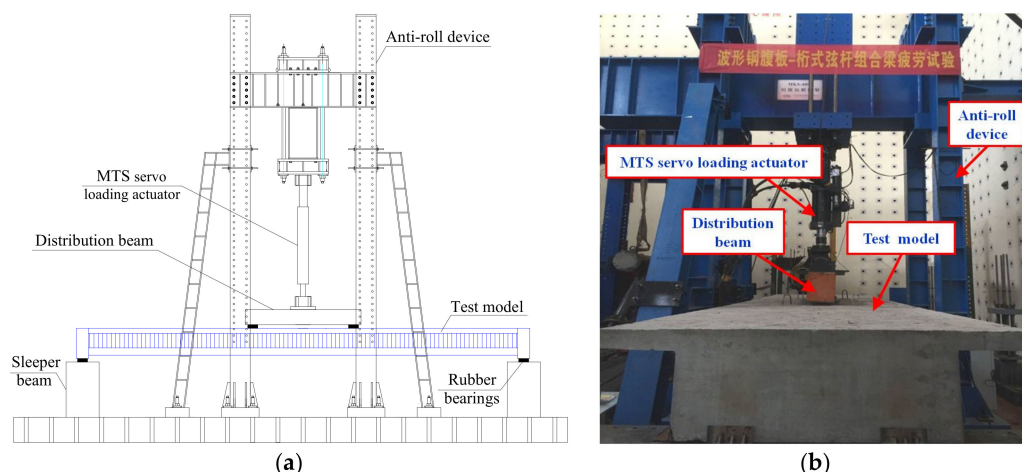


Figure 6. Loading rig: (a) schematic diagram; and (b) photo of loading rig.

According to [19], the maximum axle weight of the design vehicle is 145 kN. Considering that the overloading phenomenon is prominent in China, and the actual axle weight may be twice the design axle weight [20], for safety considerations, the fatigue load amplitude adopted in the test was taken to be 300 kN.

Combining the servo-loading actuator and the requirements for the fatigue performance tests, the lower limit of the fatigue load needs to be more than 3% of the maximum dynamic load of the actuator. Hence, the lower limits of the fatigue load adopted in the test were taken to be 50 kN.

According to the specification of the 500-kN MTS servo-loading system and the value of the fatigue load, the loading frequency was taken to be 3 Hz. The probe of the phased array ultrasonic testing system was fixed in the location with the maximum hot-spot stress to monitor the initiation of the fatigue crack uninterruptedly; meanwhile, the intersecting area between the chord and the corrugated steel webs was inspected using a magnifying glass about every 5000 cycles to verify whether a fatigue crack appeared.

The evolution of fatigue damage in composite girders with CSW-CFST truss chords with the number of load cycles was initially investigated by taking 50 kN as the load grade and 5 kN/s as the loading rate, approximately every 400,000 cycles, when cyclic loading was paused, and a static test was carried out. After fatigue crack initiation, loading was stopped, and static tests were carried out depending on the propagation process of fatigue cracks.

2.3. Instrumentation Layout of Measurement Points and Inspection Procedures

To analyze the hot-spot stress in the intersection area of the corrugated steel web and the chord, the extrapolated structural stress parallel to the weld was taken in the study as the hot-spot stress according to the relevant regulations in [21]. The extrapolation interval near the weld where the corrugated steel web intersected with the chord is shown in Table 4, in which $L_{r,\min}$ and $L_{r,\max}$ represent the minimum or maximum perpendicular distance of the unidirectional strain gauge on the gradient strain gauge away from the weld toe, respectively, and all the unidirectional strain gauges on the gradient strain gauge parallel to the weld. Figure 7 shows a gradient strain gauge specially made for this study.

Table 4. Interpolation intervals.

Monitored Parts	Chord Side	Corrugated Steel Web Side
$L_{r,\min}$ (mm)	4.0	4.0
$L_{r,\max}$ (mm)	10.0	14.0

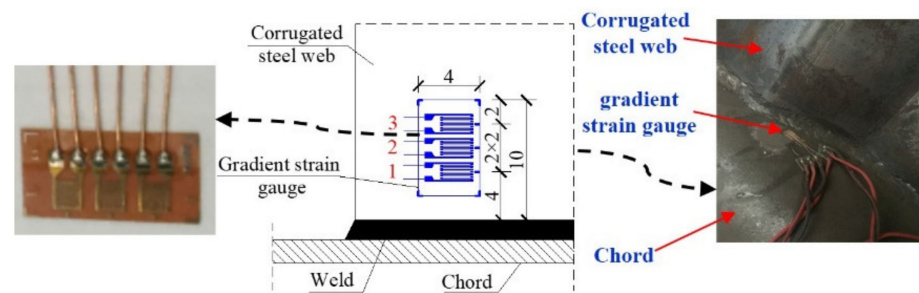


Figure 7. Gradient strain gauge (unit: mm).

According to the results of the fatigue performance test of the composite girders with CSW-ST truss chords reported in [11], the intersection of the inclined web of the corrugated steel web and circular arc transition section is not the only sensitive location for hot-spot stress, but also the key position for later fatigue crack initiation. Thus, the position was taken as the stress characteristic point of composite girders with CSW-CFST truss chords, where gradient strain gauges were arranged. In addition, two web wavelengths near the mid-span were taken as the monitoring range of hot-spot stress. Each monitoring point number was symbolically denoted as MNY-Z, where M corresponds to the chord (X) or the corrugated steel web (B), N corresponds to the left- (L) or right- (R) hand-side of the weld where the corrugated steel web and the chord intersect, Y is the gradient strain gauge number (1–8) counting in the longitudinal bridge direction, and Z corresponds to the number (1–3) of the unidirectional strain gauge arranged on the substrate of the gradient strain gauge. To monitor the changes in stiffness of the test model during the cyclic loading, displacement monitoring points were arranged at the bottom of the chord at $L/4$, $L/2$, and $3L/4$ sections, and LVDTs were used to measure displacements of the composite girders with CSW-CFST truss chords. The layout of the strain monitoring points is shown in Figure 3.

An elastic controllable synthetic wave was generated by a phased array ultrasonic testing system, which not only guaranteed high sensitivity and resolution for the detection of initial defects, but also facilitated the three-dimensional quantitative analysis of the initial defects and fatigue cracks [22]. According to the existing research results, the initial defects with the size of $0.05 \text{ mm} \times 0.05 \text{ mm}$, which cannot be detected with the naked eye, can be detected by a phased array ultrasonic testing system. Thus, a phased array ultrasonic testing system was used to conduct non-destructive tests of the intersection welds between the corrugated steel webs and the chords of the composite girders with CSW-CFST truss chords following the requirements listed in [23]. According to the results of the initial defect detection, there was no initial defect at the intersection between the corrugated steel web and the chord, thus eliminating potential influence on the results of the fatigue performance test.

3. Analysis of Fatigue Performance Results

3.1. Extrapolation Methods for Hot-Spot Stress

The methods for calculating hot-spot stress mainly include the one-point representation method [24], two-point extrapolation method [25], and three-point extrapolation method [26]. The one-point representation method directly assesses the stress measured at a point as the hot-spot stress. The two-point extrapolation method obtains the hot-spot stress by linear extrapolation to the weld end position. The three-point extrapolation method derives the hot-spot stress parabolically by extrapolation to the weld end position.

For brevity, the hot-spot stress at point XL3 with the maximum tensile stress measurement point was taken as an illustrative example. The results obtained by different calculation methods are shown in Figure 8, where the abscissa indicates the distance of the unidirectional strain gauge on the gradient strain gauge substrate from the welding toe. The hot-spot stress obtained by the one-point representation method was the smallest, and the hot-spot stress obtained by the two-point extrapolation method was slightly larger than that obtained by the three-point extrapolation method, with a difference of no more

than 3.6%. The maximum peak obtained by the three-point extrapolation method was at a distance of about 2 mm from the weld instead of at the weld, which is unreasonable. Considering structural safety and convenience, in a design situation and for evaluating the results of fatigue testing, it is advisable to use the two-point extrapolation method and one-point representative method to calculate the hot-spot stress in composite girders with CSW-CFST truss chords, respectively.

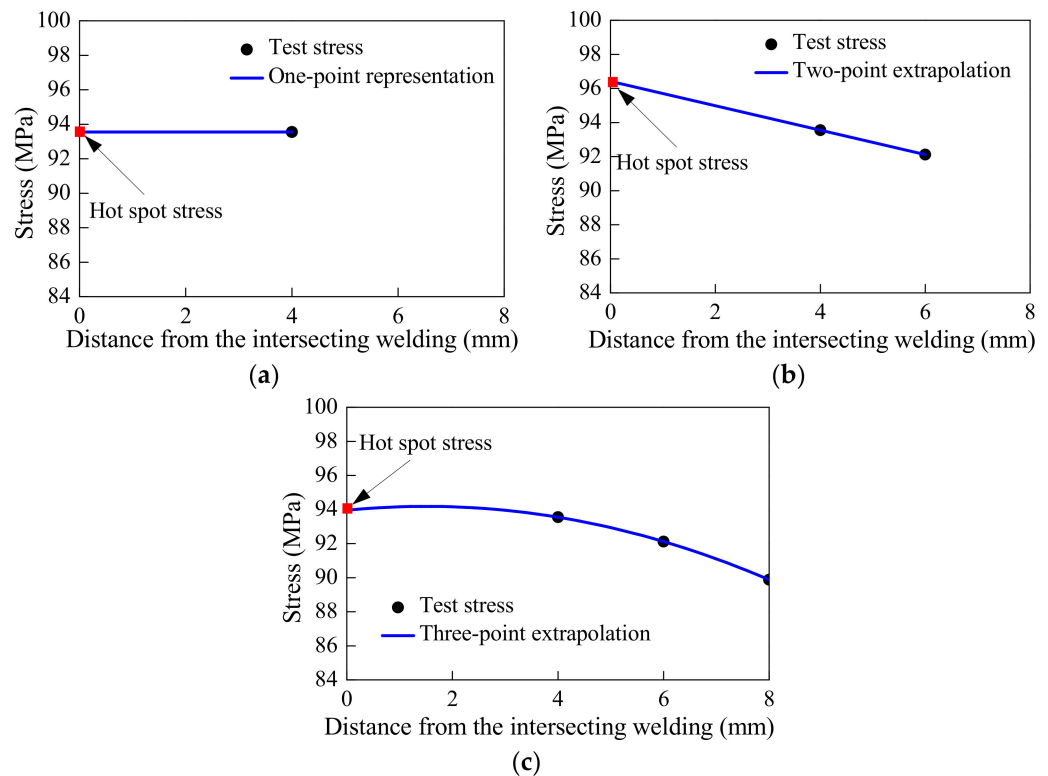


Figure 8. Comparison of hot-spot stress determination methods: (a) one-point representative method; (b) two-point extrapolation method; and (c) three-point extrapolation method.

3.2. Hot-Spot Stress Distribution

In order to improve the reliability of the test results, the stress results were taken to be the average value over multiple tests. Combining the modulus of elasticity obtained by the material property test, stresses can be obtained from the monitoring strain multiplied by the modulus of elasticity. The hot-spot stress at each key measurement point of the composite girder with CSW-CFST truss chords under peak load was calculated using the extrapolation method, as shown in Figure 9. The hot-spot stress distribution in the same chord of the composite girder with CSW-CFST truss chords was essentially symmetric with respect to the mid-span section, and the deviation was less than 4.2%. Furthermore, the hot-spot stress in the left- and right-hand-side chords essentially coincided, and the deviation was less than 7.6%. The reasons why the deviation was found include that the axis line of the composite girder was not located in the loading surface, and the left- and right-hand-side chords were not entirely parallel to each other, with some deviation existing between them. It was demonstrated that the designed test model and its boundary conditions were reasonable.

In addition, according to Figure 9, the maximum hot-spot stress position was at point S, which was the next-nearest point to the mid-span section. This was mainly because the stress measurement points were arranged on the same plane of the corrugated steel web. The nearest and next-nearest point S to the mid-span section were on the molded side and the non-molded side, respectively, which was basically the same as that of composite girders with CSW-ST truss chords in [11], indicating that concrete in the chord does not change the hot-spot stress distribution in the welded zone.

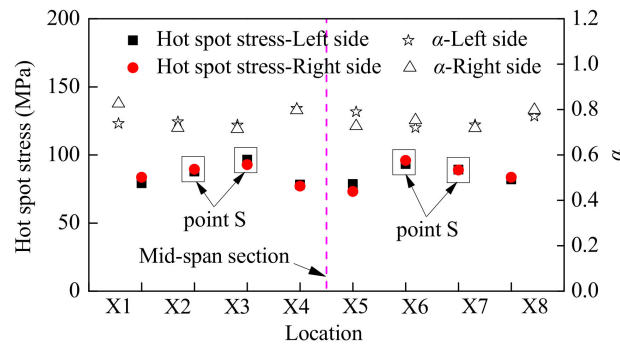


Figure 9. Distribution and comparison of hot-spot stress.

Figure 9 shows the ratios, denoted as α , of hot-spot stress in the composite girder with CSW-CFST truss chords to those in the composite girder with CSW-ST truss chords under the peak loads at the same measurement points. α was in the range from 0.732 to 0.826. α was 0.732 at the maximum hot-spot stress position, which shows that concrete in the chord reduced the hot-spot stress of the composite girder with CSW-ST truss chords by 26.8%.

3.3. Fatigue Failure Process

The test results of key strain and displacement measurement points in the composite girder with CSW-CFST truss chords, after different numbers of reversed loading cycles, are presented in Figures 10 and 11, while Figure 12 shows the time histories of strains at key measurement points. In Figure 10, the strain is the maximum value corresponding to the peak load when experiencing different numbers of reversed loading cycles. The evolution of fatigue damage using Figures 10–12 was divided into three stages: fatigue crack initiation, propagation, and failure. During the initial 2,045,000 reversed loading cycles, both strain and the displacement of any key measurement point experienced no obvious changes.

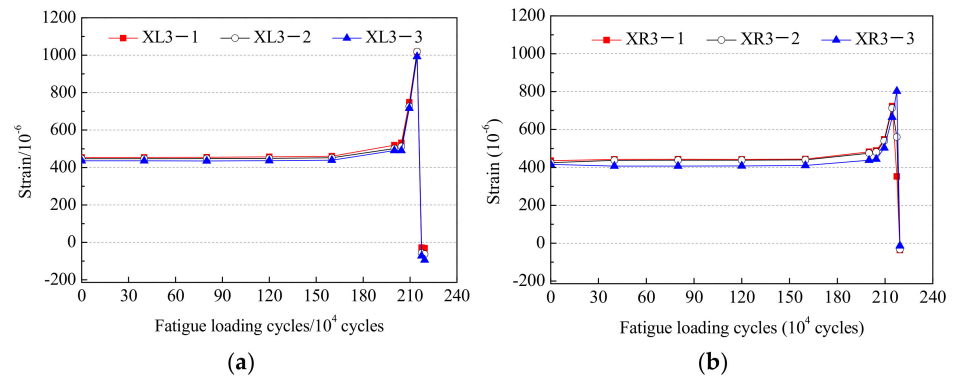


Figure 10. Fatigue loading cycles-strain curves: (a) XL3; and (b) XR3.

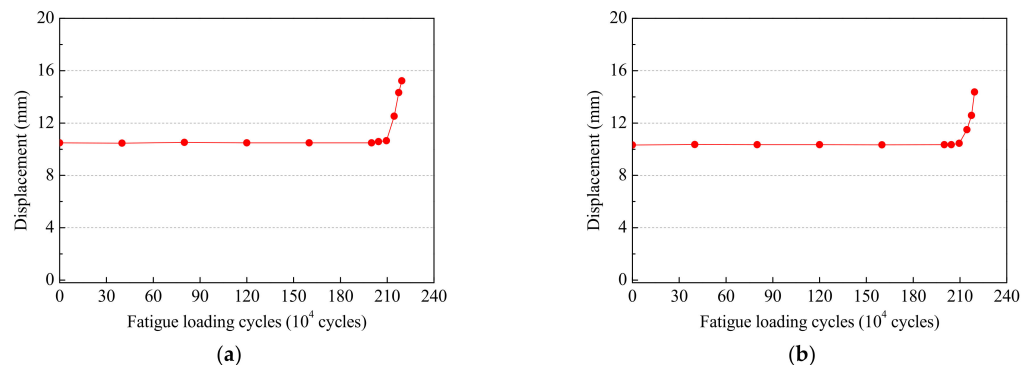


Figure 11. Fatigue loading cycles-displacement curves: (a) WL2; and (b) WR2.

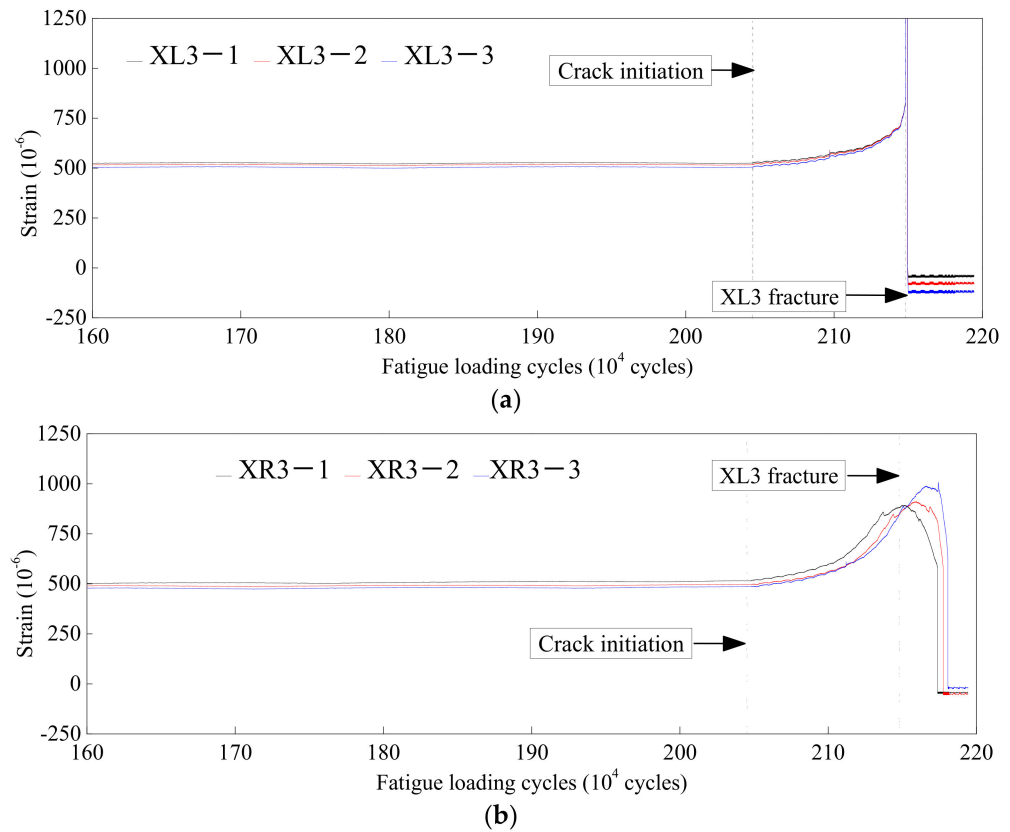


Figure 12. Time histories of strain: (a) XL3; and (b) XR3.

When the number of reversed loading cycles reached 2,045,000, both strain at XL3 and displacement at WL2 gradually started increasing with increase in the reversed loading cycles. By combining the observation with the phased array nondestructive detection, as shown in Figure 13, where C_L and h_L represent the length and the depth of the fatigue crack in the left side of the section, C_R and h_R represent the length and the depth of the fatigue crack in the right side of the section, and the red line represents the fatigue crack, it can be concluded that the girder started cracking at XL3, with the length, width and depth of fatigue crack being 0.8 mm, 0.1 mm, and 0.1 mm, respectively. The fatigue life consumed before fatigue crack initiation accounted for 93.0% of the total reversed fatigue loading cycles. Compared to that of the composite girder with CSW-ST truss chords reported in [11], concrete in the chord lengthened the service life of the composite girder with CSW-ST truss chords by about 61.5% under the action of the same fatigue load.

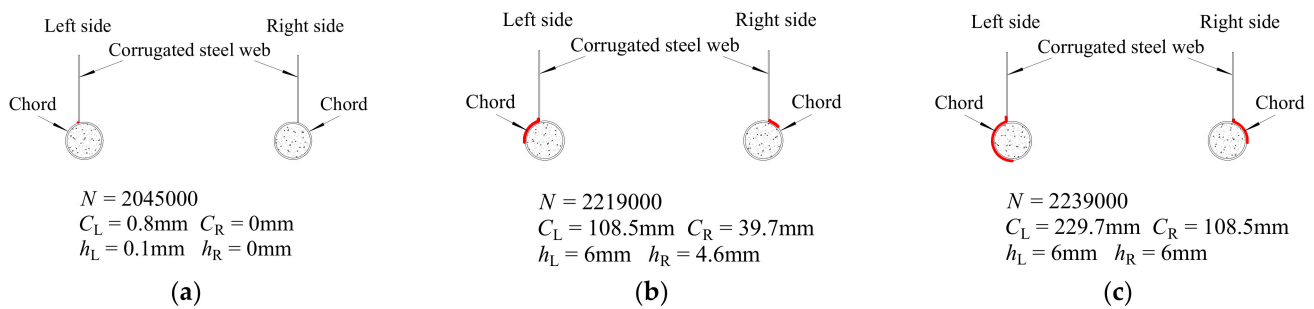


Figure 13. Fatigue crack detection results: (a) initiation; (b) propagation; and (c) failure.

When the reversed loading cycles were between 2,045,000 and 2,145,000, the strain at XL3 and displacement at WL2 grew rapidly. The time history of strain at XL3 had a point of inflection and then exhibited a stepped decline when the reversed loading cycles

reached about 2,145,000, indicating that the fatigue crack propagated through the chord wall thickness until it penetrated the wall completely.

After the reversed loading cycles exceeded 2,145,000, the fatigue crack propagated further along the circumferential direction of the corrugated steel web and the chord. After about 2,194,000 reversed loading cycles, the length of the fatigue crack reached about 269.7 mm, and it crossed the very bottom of the chord. At that time, the displacement of the composite girders also reached a maximum value (15.2 mm), which exceeded 1/600 of the calculated span length, namely 14.6 mm, indicating that the composite girder essentially lost its loading capacity and entered the fatigue failure stage.

The propagation rates of fatigue cracks in different directions can be further compared. The relationships between fatigue crack propagation depth or length and the fatigue loading cycles of the composite girder with CSW-CFST and CSW-ST truss chords are shown together in Figure 14.

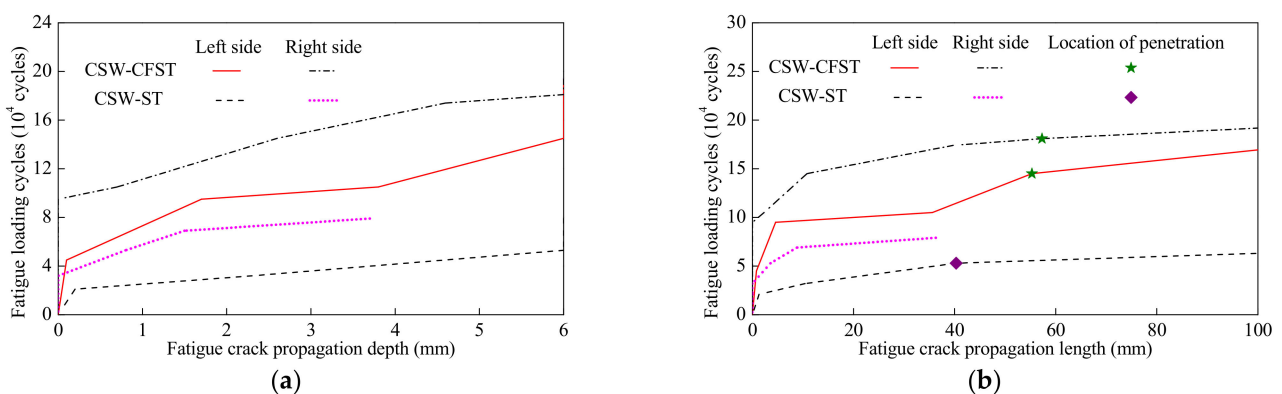


Figure 14. Comparison of fatigue crack propagation rates: (a) propagation depth-loading cycles curves; and (b) propagation length-loading cycles curves.

It can be seen in Figure 14a that the fatigue crack propagation depth-loading cycle curves of the composite girder with CSW-CFST truss chords were all above those of the composite girder with CSW-ST truss chords, indicating that, for the same fatigue load and same fatigue crack propagation depth, the reversed fatigue loading cycles borne by the composite girders with CSW-CFST truss chords were greater than that borne by the composite girder with CSW-ST truss chords.

As can be seen in Figure 14b, the propagation rates along the fatigue crack length direction in the composite girder with CSW-CFST and CSW-ST truss chords were 3.81 mm/100,000 cycles and 7.60 mm/100,000 cycles during the fatigue crack propagation stage, respectively, and those at the fatigue failure stage were 35.59 mm/100,000 cycles and 112.38 mm/100,000 cycles, respectively. Therefore, it can be concluded that, as the fatigue crack transitioned from the propagation stage into the failure stage, although the propagation rates along the length direction of both the composite girder with CSW-CFST and CSW-ST truss chords were clearly elevated, the latter was still much higher than the former.

In sum, concrete in the chord not only provided radial constraint for the chord steel, but also effectively lowered the neutral axis of the composite girder cross-section, reduced the axial stress in the chords, further reduced the hot-spot stress in the intersecting weld zone, and slowed the crack propagation rates along the depth and length directions in the CSW-CFST truss chords compared to those of CSW-ST truss chords during the fatigue crack propagation failure stages. The latter was also an important reason why the fatigue life of the composite girder with CSW-CFST truss chords was longer than that of the composite girder with CSW-ST truss chords.

According to the results obtained by the non-destructive examination of the initial defect, no initial defect appeared in the structure; thus, the fatigue crack did not start from an internal defect. The fatigue failure mode of the composite girders with CSW-CFST truss chords are shown in Figure 15. The fatigue crack developed at the intersection with

the maximum hot-spot stress, and the fatigue fracture surfaces were flush and essentially parallel to the chord cross-section. Moreover, the failure modes were generally consistent with those of the composite girder with CSW-ST truss chords reported in [11], indicating that the fatigue failure modes and fatigue crack types of the composite girder with CSW-ST truss chords were not changed by concrete-filling the chord.

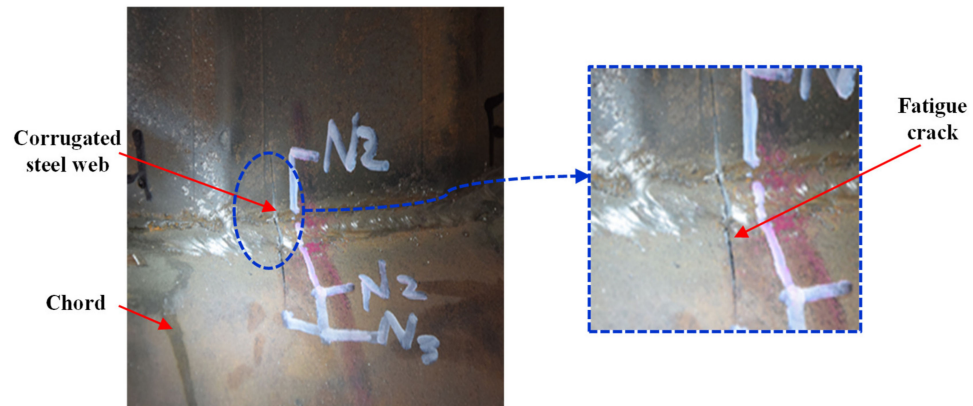


Figure 15. Fatigue failure mode.

4. Non-Linear Numerical Analysis

4.1. Non-Linear Numerical Analysis Model

A three-linear model was adopted for the tensile and compressive constitutive relationship of steel, and the typical damage plastic model considering material non-linearity was adopted for the constitutive relationship of concrete. The relevant parameters are listed in Tables 2 and 3, respectively.

A finite element model of the test specimen was constructed using MSC.MARC. The concrete bridge deck slab, the concrete in the chord, the chord, the corrugated steel webs, the cross-bracing, the K-bracing and the horizontal-bracing were all simulated with solid elements, and the rebar in the concrete bridge deck slab was simulated with truss elements. Relative slippage between the rebar and the concrete bridge deck slab and between the concrete bridge deck slab and the corrugated steel webs were ignored, and embedded and tie options were used to simulate the contact between the rebar and the concrete bridge deck slab and that between the concrete bridge deck slab and the corrugated steel web, respectively.

The interfaces between the concrete and steel were assumed to be perfectly connected without relative slip except for the interface between the chord and concrete. It was necessary to ensure a one-to-one correspondence of finite element nodes on the outer surface of concrete in the chord to those on the inner surface of the chord. These were forbidden from sharing the same nodes during the process of meshing of concrete-filling the chord to simulate the non-linear contact between the inner wall of the steel tube and the outer surface of the concrete in the chord, and to prevent occurrence of spurious sudden stress variations produced by numerical effects rather than by actual loads. The mesh of the numerical model is shown in Figure 16.

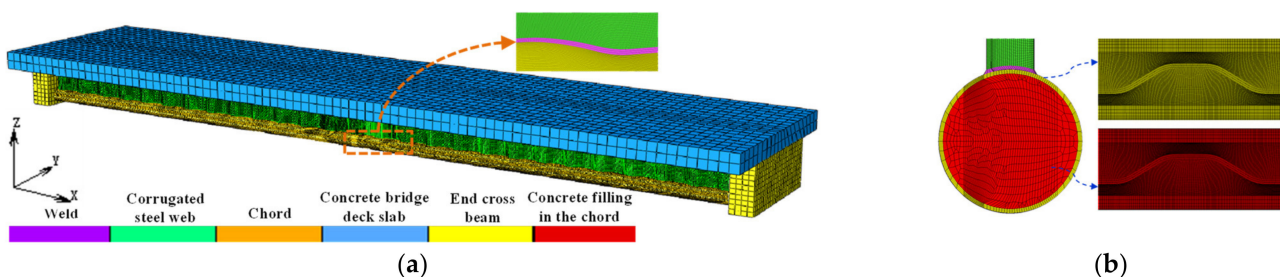


Figure 16. Mesh of numerical model: (a) entire model; and (b) concrete in chord.

The simulation of contact between the chord and concrete-filling the chord must ensure continuity of deformation and load transfer. Two main methods for non-linear simulation of contact between the chord and concrete were tried, namely, glue and touch [26]. The glue method considers that the value of the relative slippage among the components that contacted each other is zero. The touch method considers the actual relative slippage among the components that will contact each other. Comparison of results obtained with different non-linear contact simulation methods and the experimental results is shown in Figure 17. The hot-spot stress obtained with the glue contact method was markedly less than the test results. At the location with the maximum hot-spot stress, the deviation was 35.5%, indicating that the glue contact method overestimated the constraining effect of concrete in the chord, resulting in unconservative estimations. The hot-spot stress obtained by the touch contact method was in good agreement with the test results. At the position with the maximum hot-spot stress, the deviation was only 5.7%. Therefore, it is advisable to use the touch contact method to simulate the non-linear contact between the chord and concrete in the chord, and the results obtained may have a certain safety margin.

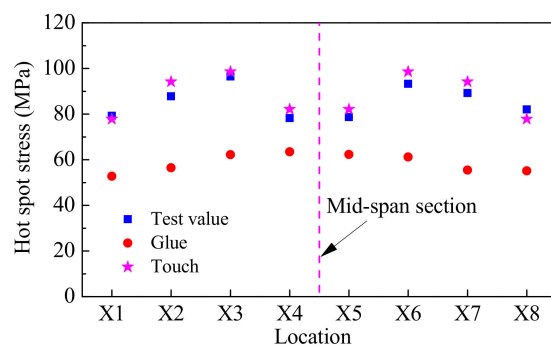


Figure 17. Comparison of different contact methods.

The boundary conditions of the non-linear numerical model simulated those of the fatigue performance test. The degrees of freedom of one end of the finite element model in the X and Z direction were constrained, and that of the other end in the Z direction were constrained. The degrees of freedom of the finite element model in the Y direction were not constrained—the finite element model could rotate freely around the X, Y and Z directions. Vertical loads symmetrical about the mid-span section were applied to the concrete deck slab. The boundary conditions of the non-linear numerical analysis model are shown in Figure 3.

Calculation accuracy is affected by the size of the mesh; thus, mesh convergence should be checked. The hot-spot stress at XL3 under different mesh sizes is shown in Figure 18. With reduction in mesh size, the hot-spot stress became gradually closer to the test value, but the accuracy was improved by only 1.3% when the mesh size was reduced from 2 mm to 1 mm. Therefore, in consideration of calculation accuracy and efficiency, as well as the thickness of the welding steel plate in the test which was 4 mm, the mesh size in the vicinity of the hot-spot in the finite element model was taken to be 2 mm. The mesh size in other regions can be enlarged.

The load-displacement curve and the hot-spot stress distribution obtained from the fatigue performance test and non-linear numerical analysis are compared in Figure 19. The load-displacement curve and hot-spot stress distribution obtained from the fatigue performance test and non-linear numerical analysis were consistent under the peak load. The deviations of the maximum displacement and the maximum hot-spot stress were less than 9.8% and 6.2%, respectively. Thus, it can be concluded that the overall performance of the actual composite girder with CSW-CFST truss chords was accurately reflected in the non-linear numerical model.

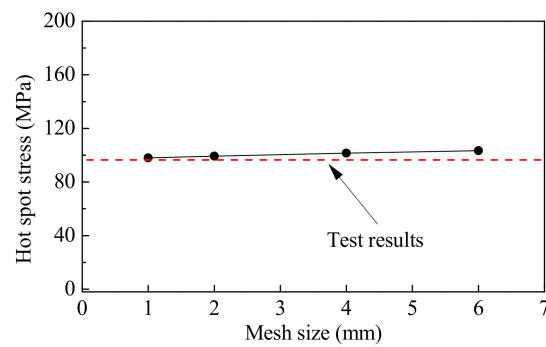


Figure 18. Mesh convergence analysis.

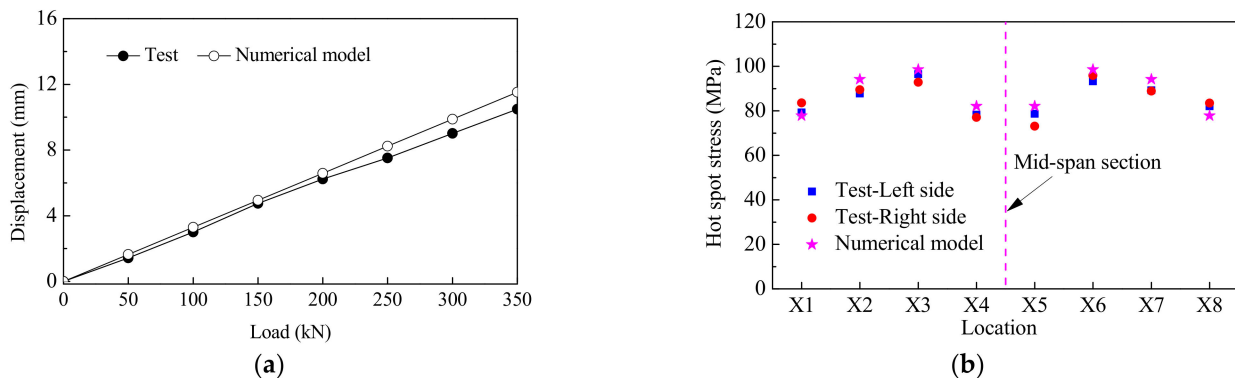


Figure 19. Accuracy verification of non-linear numerical model: (a) comparison of load-displacement curves; and (b) comparison of hot-spot stress distribution.

4.2. Sensitivity Analysis of Hot-Spot Stress

According to the test results, the hot-spot stress obtained by the two-point extrapolation method not only provides structural safety and convenience, but is more reasonable; thus, the two-point extrapolation is recommended to determine the hot-spot stress. Combining the location of the gradient strain gauge, the interval between the unidirectional strain gauge on the gradient strain gauge and the mesh size of the finite element model, and the location of the point above that was used to extrapolate the hot-spot stress, can be found in the finite element model. Then the stress on the points was extracted, and, finally, based on the extracting finite element analysis results, the hot-spot stress was obtained by two-point extrapolation.

The hot-spot stress distribution, and the maximum hot-spot stress envelopes on the left- and right-hand-sides of the intersecting weld between the corrugated steel web and the chord, are presented in Figure 20, where the origin of the horizontal axis corresponds to the mid-length section of the model. The ratio of the maximum value envelopes at the same section of the intersecting weld between the corrugated steel web and the chord in the composite girder with CSW-CFST truss chords to that in the composite girder with CSW-ST truss chords reported in [11] is given in Figure 21a, and hot-spot stress nephograms for the two types of composite girders are compared in Figure 21b.

From Figure 20, it can be seen that, for both the left- and right-hand-side of the intersecting weld, the maximum hot-spot stress occurred near point S on the non-mold pressing side. In other words, within a single wavelength, the maximum hot-spot stress at the left- and right-hand-sides of the intersecting weld did not occur at point S of the same section, and the hot-spot stress in the inclined web segment was markedly greater than that in the straight web segment.

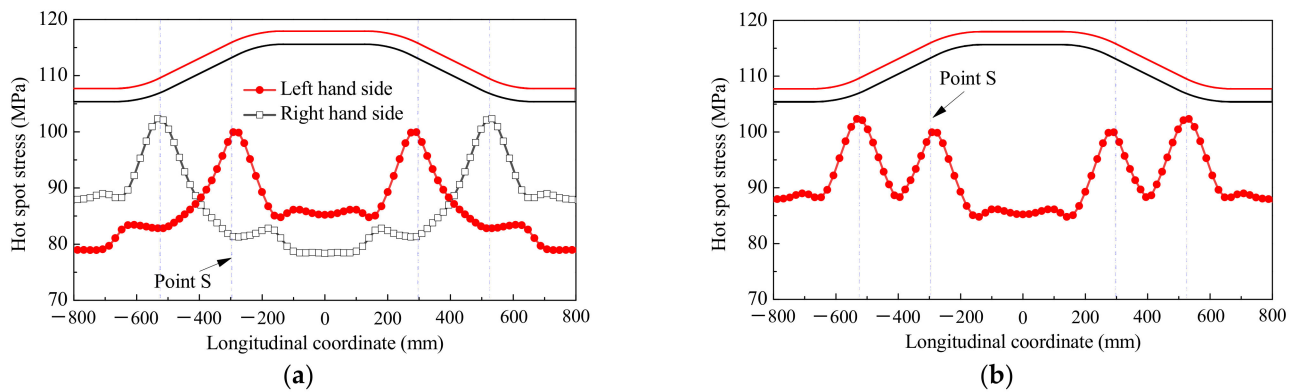


Figure 20. Analysis of hot-spot stress distribution: (a) hot-spot stress distribution; (b) envelope of hot-spot stress.

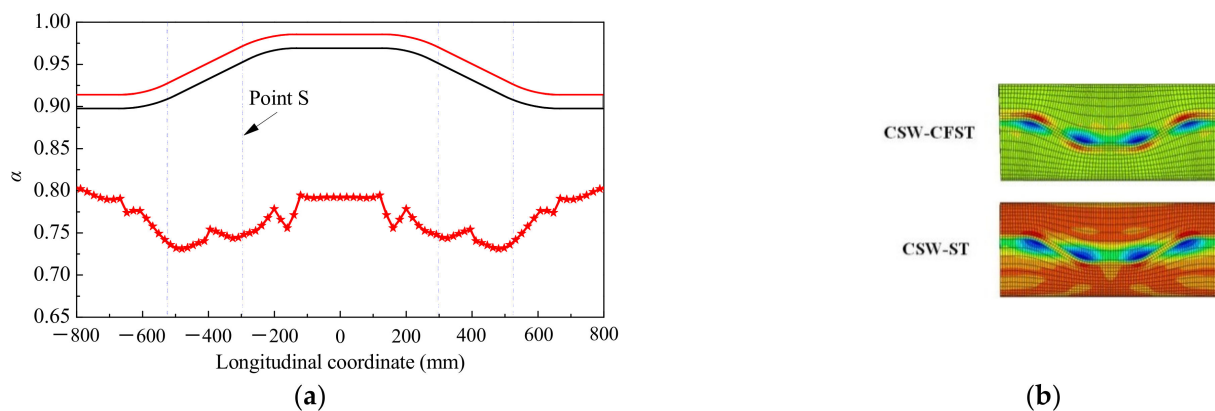


Figure 21. Influence of concrete in chord on hot-spot stress: (a) distribution of coefficient α along span length; (b) comparison of hot-spot stress nephograms.

It can be seen from Figure 21a that concrete in the chord influenced the hot-spot stress in the composite girder with the CSW-ST truss chords most obviously near the position of the maximum hot-spot stress (point S). It can be seen from Figure 20b that, compared to the composite girder with CSW-CFST truss chords subjected to the same external load, the composite girder with CSW-ST truss chords experienced a more obvious stress concentration, which occurred over a larger range, further indicating that concrete in the chord can effectively mitigate the extent of hot-spot stress concentration and improve the fatigue performance of composite girders with CSW-ST truss chords.

The parameters to be included in the analysis of the corrugated steel web are the dip angle of the inclined web (θ_w), the bend radius (R_w), and the thickness (T_w). In addition, as the chord formed the bottom of the cross-section, the diameter (D_c) and wall thickness (T_c) of the chords were also included among the parameters to be analyzed.

The values of the analytical parameters for composite girders with CSW-CFST truss chords were determined based on the sensitivity analysis of composite girders with CSW-ST truss chords carried out in [11]. To enhance the representativeness of the analysis result, the parameters used in the Maluanshan Park Viaduct in Guangdong Province, China, were taken as the benchmark model, whose dip angle of the inclined web, bend radius, and thickness of the corrugated steel web and the diameter and wall thickness were 31° , 300 mm, 20 mm, 720 mm and 20 mm, respectively. Combining the requirements of the value of the parameters in construction, a sensitivity analysis of hot-spot stress was carried out using a single variable method.

To analyze the influence of concrete in the chord on the hot-spot stress of composite girders with CSW-ST truss chords, which was the focus of the analysis, while ignoring irrelevant details, the location with the maximum hot-spot stress within a single wavelength

of the mid-span section subjected to pure bending was taken for analysis. Each individual geometric parameter was varied in turn, while keeping the other parameters unchanged, to analyze the ratio of hot-spot stress in the composite girder with CSW-CFST truss chords to that in the composite girder with CSW-ST truss chords.

The sensitivities of the ratio of hot-spot stress in the composite girder with CSW-CFST truss chords to that in the composite girder with CSW-ST truss chords to the chord diameter and chord wall thickness, thickness of the corrugated steel webs, and transition curve radius and dip angle of the corrugated steel web were analyzed, as presented in Figure 22. It can be seen from Figure 22 that the changes in the hot-spot stress in the composite girder with CSW-CFST truss chords resulting from changing any single geometric parameter essentially paralleled those in the composite girder with CSW-ST truss chords, and the variation range of α was 0.399–0.815, demonstrating that concrete in the chords reduced the hot-spot stress in composite girders with CSW-ST truss chords by 18.5–60.1%.

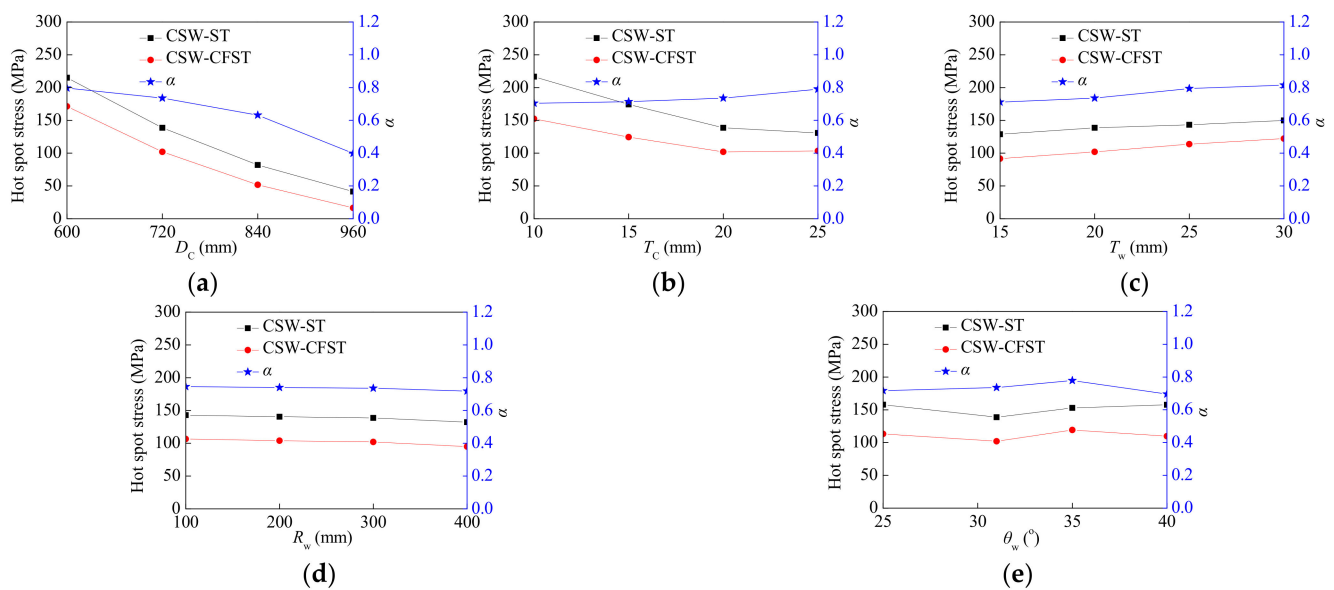


Figure 22. Sensitivity of hot-spot stress at point S to geometric parameters: (a) chord diameter; (b) chord wall thickness; (c) corrugated steel web thickness; (d) transition curve radius; and (e) corrugated steel web dip angle.

It can be seen from Figure 22a that coefficient α was negatively correlated with the chord diameter. With increase in the chord diameter, the sectional area of concrete in the chord accounted for an increasing proportion of the whole cross-sectional area of the chord. As a result, the position of the neutral axis of the cross-section moved towards the axes of the chords. Moreover, concrete in the chords participated in force, which reduced the axial stress borne by the chord steel. Therefore, the reduction rate of coefficient α gradually accelerated with increase in the chord diameter.

When only the chord thickness was changed by the same amount, the ratio of axial rigidity of the interface between the corrugated steel web and the chord to the radial rigidity of the chord in composite girders with CSW-ST truss chords was affected by the change in the chord thickness more significantly than that in composite girders with CSW-CFST truss chords. However, when only the thickness of the corrugated steel web was changed by the same change ratio, the change in the thickness of the corrugated steel web had a greater influence on the ratio of axial rigidity of the interface between the corrugated steel web and the chord to the radial rigidity of the chord in composite girders with CSW-ST truss chords than on that in composite girders with CSW-CFST truss chords. Therefore, as can be seen from Figure 22b,c, coefficient α was positively correlated with both the chord thickness and the corrugated steel web thickness.

Although the sharp-corner stress at the intersection between the inclined and straight portions of the corrugated steel web could be further relieved and the stress flow made to transition more smoothly between the two by increasing the bend radius of the corrugated steel web, the axial rigidity of the interface between the corrugated steel web and the chord or the radial rigidity of the chord could not be effectively improved; thus, α was weakly sensitive to the bend radius, as shown in Figure 22d.

Although increasing the dip angle of the inclined web can potentially improve the out-of-plane flexural rigidity and weaken the influence of the out-of-plane bending moment on the hot-spot stress, increasing the dip angle of the inclined web elevated the hot-spot stress while enhancing the axial stiffness of the interface between the corrugated steel web and the chord. Furthermore, compared to the thickness of the corrugated steel web, when only the dip angle of the web was changed by the same change ratio, this change influenced the ratio of the axial rigidity of the interface between the corrugated steel web and the chord to the radial rigidity of the chord in the composite girder with CSW-ST truss chords to a greater extent than in the composite girder with CSW-CFST truss chords. Therefore, the influence of the inclined web on coefficient α was ascribed to the coupling action of the out-of-plane flexural rigidity and the axial rigidity of the interface between the corrugated steel web and the chord. That is, coefficient α had a non-monotonic relationship with the dip angle of the web, as shown in Figure 22e.

5. Fatigue Life Evaluation Method

5.1. Definition of Fatigue Life

Five methods for experimentally determining the fatigue life of welded steel structures are summarized in DNV [27], namely: (1) the number of repeated fatigue loading cycles until the initiation of fatigue cracks, (2) the number of repeated fatigue loading cycles when the variation in strain at the most unfavorable location reaches 15% of peak dynamic strain, (3) the number of repeated fatigue loading cycles when the length of the fatigue crack reaches 30 mm, (4) the number of repeated fatigue loading cycles when the fatigue crack penetrates through the wall thickness for the first time, and (5) the number of repeated fatigue loading cycles when the test is stopped.

All these methods require physical testing or monitoring, but, compared with methods 2–5, method 1 has the most distinctive features and can be easiest to obtain. Additionally, since the fatigue life consumed during the crack propagation stage is not considered in method 1, the assessed fatigue life has a certain safety margin and conforms to the design requirements of the related Chinese specifications for the fatigue life of composite girders with CSW-CFST truss chords [17]. In consequence, method 1 was adopted in this study to determine the fatigue life of the composite girder with CSW-CFST truss chords.

5.2. Fatigue Design S-N Curve

The construction details of the welds in some cross-sections of composite girders with CSW-CFST truss chords and tubular joints are shown in Figure 23, respectively. By combining Figure 23, it can be seen that the construction details of the welds in composite girders with CSW-CFST truss chords and the tubular joints are the same, being T-shaped welds; thus, the evaluation of the fatigue life of composite girders with CSW-CFST truss chords can refer to that used in the tubular joints.

The calculated fatigue life of composite girders with CSW-CFST truss chords by the universal fatigue design S-N curve [12,21,24,27,28] is shown in Figure 24. It can be seen that the fatigue design S-N curve, which is suitable for composite girders with CSW-ST truss chords, is not suitable for composite girders with CSW-CFST truss chords. By combining Figure 24 and the measured fatigue life, it can be seen that the calculated fatigue life of composite girders with CSW-CFST truss chords obtained by the fatigue design S-N curve given in API [28] was closest to that acquired by the fatigue performance test, and the deviation was less than 17.4%. The calculated fatigue life above is less than that acquired by the fatigue performance test; that is, the evaluation adopting the fatigue design S-N

curve given in API has some redundancy. Thus, under the condition that there is no fatigue design S-N curve with higher accuracy, the fatigue design S-N curve given in API can be used to evaluate the fatigue life of composite girders with CSW-CFST truss chords.

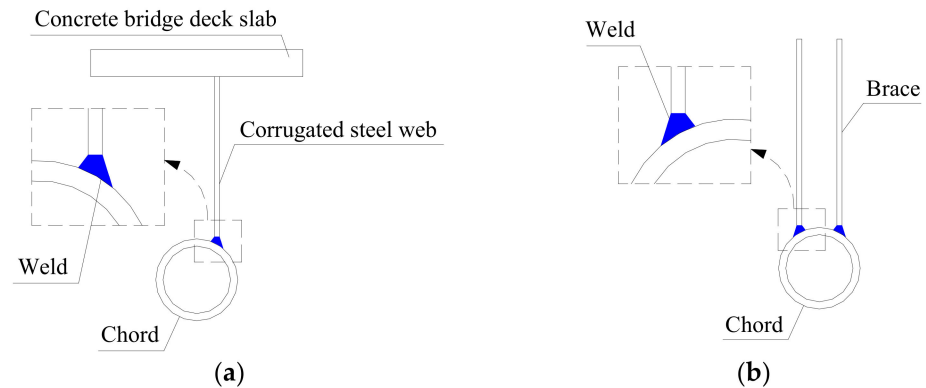


Figure 23. Comparison of welding details: (a) welding between the corrugated steel web and the chord; and (b) welding between the brace and the chord.

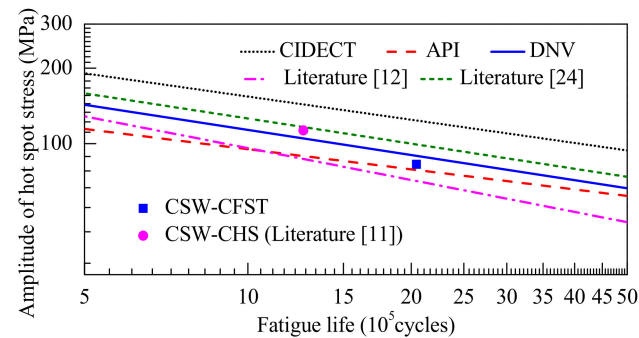


Figure 24. Comparison of measured and calculated fatigue lives.

6. Conclusions

- (1) The fatigue performance test conducted on a composite girder with CSW-CFST truss chords demonstrated that the hot-spot stress in a composite girder with CSW-CFST and CSW-ST truss chords can be obtained by the two-point extrapolation method. The extrapolation interval and measurement point layout can be determined from the CIDECT specifications. The maximum hot-spot stress position was at point S, which was the next-nearest point to the mid-span section.
- (2) The maximum hot-spot stress at the left- and right-hand-sides of the intersecting weld did not occur at point S of the same section, and the hot-spot stress in the inclined web segment was markedly greater than that in the straight web segment.
- (3) When the chord is filled with concrete, the hot-spot stress distribution in the intersecting weld zone between the corrugated steel web and the chord is more uniform. The maximum hot-spot stress of a composite girder with CSW-CFST truss chords can be decreased by 18.5% to 60.1% of that of composite girders with CSW-ST truss chords.
- (4) Under the same fatigue load, concrete in the chord increased the fatigue life by 61.5% compared to composite girders with CSW-ST truss chords. The fatigue crack growth rates of the composite girder with CSW-CFST truss chords along both depth and length directions were slower than those of the composite girder with CSW-ST truss chords during crack propagation and failure stages.
- (5) Based on the existing fatigue design S-N curve, it was found that when there is no fatigue design S-N curve with higher accuracy, the fatigue design S-N curve given in API can be used to evaluate the fatigue life of composite girders with CSW-CFST truss chords, and the deviation is less than 17.4%.

Author Contributions: H.H., K.C., Q.W. and S.N. conceived and designed the experiments; H.H. and K.C. performed the experiments and analyzed the data; K.C., and Q.W. contributed reagents/materials/analysis tools; and H.H. wrote the paper. All authors have read and agreed to the published version of the manuscript.

Funding: This research was funded by the National Key Research and Development Program of China (No. 2017YFE0130300), National Natural Science Foundation of China (No. 52078137), and Natural Science Foundation of Fujian Province (No. 2019J06009).

Data Availability Statement: The data generated or used during the study are included within the submitted article.

Acknowledgments: The tests were conducted at the Fujian Provincial Key Laboratory on Multi-Disaster Prevention and Mitigation in Civil Engineering at Fuzhou University. The support provided by the laboratory staff is gratefully acknowledged.

Conflicts of Interest: The authors declare no conflict of interest.

References

1. Chen, Y.Y.; Dong, J.C.; Tong, Z.J.; Jiang, R.J.; Yue, Y. Flexural behavior of composite box girders with corrugated steel webs and trusses. *Eng. Struct.* **2020**, *209*, 1–10. [[CrossRef](#)]
2. Chen, Y.Y.; Dong, J.C.; Xu, T.H. Composite box girder with corrugated steel webs and trusses—A new type of bridge structure. *Eng. Struct.* **2018**, *166*, 354–362. [[CrossRef](#)]
3. Dong, J.C.; Chen, Y.Y.; Wu, Q.X.; Hu, A.X.; Jiang, R.J.; Wang, C.W.; Tong, Z.J.; Song, H.; Xu, T.H. Research on flexural behavior of composite box continuous girder with corrugated steel webs and trusses. *Adv. Struct. Eng.* **2021**, *24*, 3580–3593. [[CrossRef](#)]
4. Jiang, R.J.; Wu, Q.M.; Xu, T.H. Effective flange width for composite box girder with corrugated steel webs. In Proceedings of the 2016 Structures Congress (Structures16), Jeju, Korea, 28 August–1 September 2016.
5. Huang, W.; Fenu, L.; Chen, B.; Briseghella, B. Experimental study on joint resistance and failure modes of concrete filled steel tubular (CFST) truss girders. *J. Constr. Steel Res.* **2018**, *141*, 241–250. [[CrossRef](#)]
6. Chen, Y.Y.; Dong, J.C.; Xu, T.H.; Xiao, Y.F.; Jiang, R.J.; Nie, X.M. The shear-lag effect of composite box girder bridges with corrugated steel webs and trusses. *Eng. Struct.* **2019**, *181*, 617–628. [[CrossRef](#)]
7. Dong, J.C. Research on Mechanical Performance of Composite Box-Girder Bridges with Corrugated Steel Web and Chords. Ph.D. Thesis, Fuzhou University, Fuzhou, China, 2017.
8. Wang, C.W. Research on the Bending Behavior of CSW-CFST Truss-Chord Continuous Girder. Master's Thesis, Fuzhou University, Fuzhou, China, 2017.
9. Pan, Y.Z. Study on Mechanical Behavior of Composite Beam Bridge with Corrugated Steel Webs and Concrete Filled Steel Tube under Vehicle Load. Master's Thesis, Fuzhou University, Fuzhou, China, 2020.
10. Huang, J.Y. Research on the Bending and Torsion of Composite Beams with Corrugated Steel Web. Master's Thesis, Fuzhou University, Fuzhou, China, 2019.
11. Lin, Q.H. Experimental Research on Fatigue Performance of Composite Girders with CWS-ST Truss Chords. Master's Thesis, Fuzhou University, Fuzhou, China, 2018.
12. Wei, X.; Wen, Z.Y.; Xiao, L.; Wu, C.T. Review of fatigue assessment approaches for tubular joints in CFST trusses. *Int. J. Fatigue* **2018**, *113*, 43–53. [[CrossRef](#)]
13. Zheng, J.; Nakamura, S.; Okumatsu, T.; Nishikawa, T. Formulation of stress concentration factors for concrete-filled steel tubular (CFST) K-joints under three loading conditions without shear forces. *Eng. Struct.* **2019**, *190*, 90–100. [[CrossRef](#)]
14. Musa, I.A.; Mashiri, F.R. Stress concentration factor in concrete-filled steel tubular K-joints under balanced axial load. *Thin-Walled Struct.* **2019**, *139*, 186–195. [[CrossRef](#)]
15. Xu, F.; Chen, J.; Jin, W. Experimental investigation of SCF distribution for thin-walled concrete-filled CHS joints under axial tension loading. *Thin-Walled Struct.* **2015**, *93*, 149–157. [[CrossRef](#)]
16. Musa, I.A.; Mashiri, F.R.; Zhu, X. Parametric study and equation of the maximum SCF for concrete filled steel tubular T-joints under axial tension. *Thin-Walled Struct.* **2018**, *129*, 145–156. [[CrossRef](#)]
17. IIW: 1996. *Fatigue Design of Welded Joints and Components*; Abington Publishing: Cambridge, UK, 1996.
18. Elamary, A.S.; Alharthi, Y.; Abdalla, O.; Alqurashi, M.; Sharaky, I.A. Failure mechanism of hybrid steel beams with trapezoidal corrugated-web non-welded inclined folds. *Materials* **2021**, *14*, 1424. [[CrossRef](#)] [[PubMed](#)]
19. Chen, B.; Ye, Z.N.; Chen, Z.S.; Xie, X. Bridge vehicle load model on different grades of roads in China based on Weigh-in-Motion (WIM) data. *Measurement* **2018**, *122*, 670–678. [[CrossRef](#)]
20. Chen, K.M.; Huang, H.H.; Wu, Q.X.; Nakamura, S.; Chen, B.C. Experimental and finite element analysis research on the fatigue performance of CHS K-joints. *Eng. Struct.* **2019**, *197*, 1–14. [[CrossRef](#)]
21. CIDECT: 2001. *Part 8: Design Guide for Circular and Rectangular Hollow Section Joints under Fatigue Loading*; TÜV-Verlag GmbH: Köln/Berlin, Germany, 2001.

22. Zhou, Y.L.; Qian, X.D.; Birnie, A.; Zhao, X.L. A reference free ultrasonic phased array to identify surface cracks in welded steel pipes based on transmissibility. *Int. J. Press. Vessel. Pip.* **2018**, *168*, 66–78. [[CrossRef](#)]
23. Qian, X.D.; Swaddiwudhipong, S.; Nguyen, C.T.; Petchdemanengam, Y.; Marshall, P.; Ou, Z. Overload effect on the fatigue crack propagation in large-scale tubular joints. *Fatigue Fract. Eng. Mater. Struct.* **2013**, *36*, 427–438. [[CrossRef](#)]
24. JSSC: 1995. *Fatigue Design Recommendations for Steel Structures*; Jihodobooks: Tokyo, Japan, 1995.
25. Shao, Y.B.; Du, Z.F.; Lie, S.T. Prediction of hot spot stress distribution for tubular K-joints under basic loadings. *J. Constr. Steel Res.* **2009**, *65*, 2011–2026. [[CrossRef](#)]
26. Zheng, J.; Nakamura, S.; Ge, Y.; Chen, K.M. Extended Formulation of Stress Concentration Factors for CFST T-Joints. *J. Bridge Eng.* **2020**, *25*, 1–5. [[CrossRef](#)]
27. DNV-RP-C203: 2005. *Fatigue Design of Offshore Steel Structures*; DNV Services: Høvik, Norway, 2008.
28. API: 2002. *Recommended Practice for Planning, Designing, and Constructing Fixed Offshore Platforms Working Stress Design*; API Publishing Services: Washington, DC, USA, 2002.